



Monitoring of Stresses in Concrete Using Ultrasonic Coda Wave Comparison Technique

Ali Hafiz¹ · Thomas Schumacher¹

Received: 4 February 2018 / Accepted: 14 September 2018 / Published online: 21 September 2018
© Springer Science+Business Media, LLC, part of Springer Nature 2018

Abstract

Condition or health monitoring of concrete structures has experienced increasing interest over the last decade. While conventional sensors such as strain gauges are accurate and reliable, they only allow for surface observations. In contrast, ultrasonic waves propagate through the thickness of a member and can thus detect internal changes. In this paper we present an ultrasonic monitoring approach that uses a coda wave comparison (CWC) technique, which makes use of the highly sensitive diffuse (or coda) portion of a recorded ultrasonic waveform. In this study, the changes in the applied stress were correlated to the changes observed in the ultrasonic waveforms, which were estimated using magnitude-squared coherence (MSC). The CWC technique was evaluated by investigating key influence parameters that affect the relationship between MSC and the applied stress. First, two concrete cylinders were cast and tested to study the effect of maximum aggregate size. Second, two concrete prisms were used to study the effect of the frequency of the transmitted pulse. Finally, we discuss a field test involving a prestressed concrete bridge girder and a column. The results show that MSC is capable of discriminating minute stress changes in a laboratory as well as a field setting.

Keywords Ultrasound · Coda wave comparison · Concrete · Stress · Magnitude-squared coherence

1 Introduction

Concrete is the most widely used building material in the world [1]. Monitoring the performance of concrete structures has increased in the last two decades [2] due to aging and deterioration and limited funds available for maintenance and repair. Structural health monitoring provides a range of useful information related to the short and long-term performance of a structure such as changes in stress, ongoing cracking, chloride levels, corrosion potential, etc. This information can support maintenance and repair decisions and may also help improving design and construction standards.

Overloading and fatigue are the most common causes of cracking in concrete structures and may lead to deterioration such as rebar corrosion. Therefore, monitoring the stress conditions in concrete members provides important information

regarding structural performance. A number of sensors have been developed to monitor stress conditions, such as strain gauges, accelerometers, or displacement sensors, etc. All of these sensors are attached to the surface and, therefore, they only represent a surface observation. Another limit of these sensors is that they can measure stress only at the point of their location. While distributed sensors exist, they are still bound to the surface. Ultrasonic stress waves have also been found to be sensitive to changes in stress and an advantage over traditional sensors as they travel through the thickness of a member. The challenge lies in the interpretation of the signals, i.e. how changes in the recorded signals are related to changes in stress.

Hughes and Kelly [3] established a relationship between the p-wave velocity of ultrasonic waves and the applied stress inside a solid material, after third-order elastic constants were introduced by Murnaghan [4]. In concrete, this theory is not directly applicable since the variation in time of flight (TOF) (or the propagation velocity) is extremely minute and, thus, difficult to measure [4–6]. For example, our previous experiment on a small concrete cylinder did not show any change in p-wave velocity until the applied stress reached 60% of ultimate stress [7]. This represents a significant level of stress

✉ Thomas Schumacher
thomas.schumacher@pdx.edu

Ali Hafiz
hafiz@pdx.edu

¹ Civil and Environmental Engineering, Portland State University, 1930 SW 4th Avenue, Portland, OR 97201, USA

and is well above a typical service-level or cracking stress. Therefore, we have been further investigating the evaluation of the diffuse portion of the ultrasonic signals.

Concrete is a heterogeneous material and is made up of different sizes of materials, such as gravel, sand, and cement paste. Due to this heterogeneity, the ultrasonic stress wave experiences multiple scattering during propagation, making the signal more complex [8]. Generally, an ultrasonic signal can be divided into two portions: the coherent (early portion containing p-wave arrival) and the diffuse (late portion or coda wave) portion. As discussed earlier, the coherent portion is not sensitive to a change in the applied stress. On the other hand, any small change in the material has an effect on the coda wave, such as amplitude, energy, and the local phase [9].

The term coda wave originates from the field of geophysics [10], and has been used in materials science for the last decade. A common technique used in this field is called coda wave interferometry (CWI). A number of applications based on CWI for monitoring changes in concrete have been reported [5]. In addition to using CWI for monitoring stress, it has been used to monitor cracking [8, 10–12], temperature changes [13–15], and ASR [16]. Typically, the time lag between coda wave signals is estimated by applying cross correlation [5]:

$$CC(t, \delta t) = \frac{\int_{t_1}^{t_2} Y_0[t]Y_i[t + \delta t]dt}{\sqrt{\int_{t_1}^{t_2} Y_0^2 dt \int_{t_1}^{t_2} Y_i^2 dt}} \quad (1)$$

where Y_0 and Y_i is the waveform in the initial and final state, respectively, and (t_1, t_2) is the time window in the coda wave. CWI is much more sensitive than TOF to stress changes in concrete [17]. In addition, the sensitivity of CWI velocities relates to direction of the load respect to direction of wave propagation where the parallel situation shows greater sensitivity [18]. CWI has been successfully used for monitoring stresses in a concrete beam tested under a four-point bending load [1]. In addition, CWI was used to determine the non-linear constants for concrete by obtaining the relative velocity change for a concrete cylinder [19]. Stähler et al. [6] estimated the stress changes in an existing bridge by using CWI. Zhang et al. [2] used the CWI to correlate the velocity change in coda wave with the applied tensile stress in a concrete cylinder. Moreover, CWI and nonlinear acoustic waves can provide potential field applicability for in situ measurements because of their sensitivity to the microstructural changes in concrete [20]. Questions exist regarding sampling frequency and the type of windowing technique to employ when performing CWI. Since the relative change in velocity is small, a high sampling frequency is required. Sometimes, a sampling frequency of 10 MHz is still not enough to detect a change in stress. The location, length, and number of time

windows vary from study to study and no recommendations exist for using a specific time window. Liu et al. [21] applied the Taylor series expansion method on coda waves of a concrete cylinder to avoid signal resampling and time consuming calculations in the traditional CWI analysis.

Over the last decade, the interest in quantifying the similarity between signals has increased. Larose et al. [22] proposed a decorrelation coefficient (K) by using the correlation coefficient as shown in Eq. (2). The decorrelation coefficient was used to measure the change in the similarity of the coda wave due to the evolution of cracks inside concrete. Based on the decorrelation coefficient and CWI, the researchers developed the LOCADIFF technique for crack imaging [23].

$$K = 1 - \frac{\int_{t_1}^{t_2} Y_0[t]Y_i[t]dt}{\sqrt{\int_{t_1}^{t_2} Y_0^2 dt \int_{t_1}^{t_2} Y_i^2 dt}} \quad (2)$$

Niederleithinger et al. [24] applied the squared correlation coefficient (R^2) on a time window in the coda wave and related it with applied stress. The authors of this paper also correlated the R^2 with applied stress, but they used the entire (or full) waveforms [7]. They also used magnitude-squared coherence (MSC) to compute the similarity between full-waveforms, where MSC was correlated with applied stress in concrete cylinders [25]. Grosse [26] originally proposed the use of MSC to compare acoustic emission (AE) signals. Finally, Chen and Schumacher [27] applied MSC on the coda wave to correlate it with the length of a notch in a steel plate.

Environmental parameters such as temperature and humidity have been found to have a significant effect on the coda wave portion, and structures such as bridges are fully exposed to environment [28]. Yuxiang Zhang et al. [29] proposed a thermal bias control technique by using a second (reference) specimen. They concluded that their technique could reduce the bias from both stress effects and environmental temperature fluctuations [29]. Fröjd and Ulriksen [28] used the Mahalanobis distance to distinguish between signal changes stemming from damage and the environment.

2 Research Significance

This paper proposes a coda wave comparison (CWC) technique based on magnitude-squared coherence (MSC) of ultrasonic signals for monitoring internal stresses in concrete. In this technique, the entire recorded ultrasonic waveform is used, not relying on an arbitrary window. Through a series of laboratory experiments, the proposed technique was found capable of discriminating minute changes in the internal stress in concrete. Additionally, the methodology was evaluated during an in-service bridge load test where the MSC value correlated directly with the internal forces of the tested

members. In conclusion, ultrasonic monitoring in conjunction with CWC represents a promising technique to monitor internal stresses. In this study, the environmental effects were minimal and therefore not considered since the testing time was only on the order of a few minutes.

3 Methodology

3.1 Monitoring Methodology

Our proposed monitoring methodology is based on ultrasonic stress wave measurements, which are taken at selected intervals. Figure 1 illustrates the fundamental idea on a simple setup with one transmitting (T) and one receiving (R) piezoelectric transducer. The option exists to employ a network of sensors, which would allow for spatial discrimination of changes. While the transmitted pulse is selected by the operator and thus assumed to be constant, the received (or recorded) waveforms will change if the material experiences an internal change. This approach is different from the acoustic emission (AE) monitoring technique in that it is an active process. AE monitoring is passive and records stress waves released due to sudden processes such as cracking or friction.

Subsequently, a mathematical framework is presented for our proposed monitoring approach and a waveform comparison technique that allows monitoring for minute and slowly varying changes in concrete.

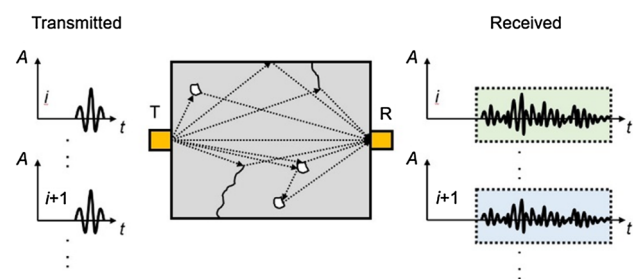


Fig. 1 Illustration of proposed ultrasonic monitoring methodology. Only one transmitting (T) and one receiving (R) transducer are shown for simplicity

3.2 Coda Wave Comparison

Our proposed coda wave comparison (CWC) technique attempts to correlate observed changes in recorded ultrasonic signals with internal structural changes that develop in concrete. This paper focuses on the changes that manifest due to changes in the interior stresses. In this technique, the entire waveform, including both the first arrival and the coda portion of the wave, is used in order to avoid having to select an arbitrary window. The measurements performed in this tech-

nique can be mathematically described using a signals and system’s framework as a measurement chain of the following form [30]:

$$R(t) = S(t) * TF_G(t) * TF_T(t) * TF_{DAQ}(t) \tag{3}$$

where $R(t)$ is the recorded digitized signal, $S(t)$ describes the transmitted pulse (i.e. source), $TF_G(t)$ is the Green’s function describing stress wave propagation effects in the medium, and $TF_T(t)$ and $TF_{DAQ}(t)$ are the impulse responses of the transducers and the data acquisition unit, respectively. The four elements are linked in the time domain via convolution, which is denoted as “*”. When high-fidelity components are used that have a flat response over the range of frequencies of interest, the respective element in the measurement chain has a theoretical value of $TF_x(t) = 1$, which means it can be neglected. Assuming that high-fidelity system components are used, and the coupling of the transducers does not change over time, Eq. (3) reduces to:

$$R(t) = S(t) * TF_G(t) \tag{4}$$

In the case of our proposed ultrasonic monitoring approach, $S(t)$ does not change over time, and we can therefore attribute the observed differences between measurements, $R(t)$, solely with changes in the Green’s function, $TF_G(t)$, and hence with changes occurring in the material. The changes in the interior stresses cause minute relocations of the aggregates and eventually micro cracking, which affect the propagation of stress waves through the concrete. This has a particular influence on the coda portion due to the multiple scattering effect seen in concrete, resulting in a change of amplitudes, time shifts, and alteration of frequency content. Mathematically, these changes may be presented as follows:

$$\Delta TF_G(t) \propto \Delta\sigma \tag{5}$$

where $\Delta TF_G(t)$ represents the changes inside the concrete resulting from changes in the interior stress, $\Delta\sigma$. Although micro cracks are randomly generated, we can assume they follow a normal distribution in the propagation path of the stress wave. Also, a change in the location of an aggregate is assumed to linearly correlate with interior stress. Therefore, we can assume the changes in concrete vary linearly with stress. Using this assumption and substituting Eq. (5) into Eq. (4) we get:

$$\Delta R(t) \propto \Delta\sigma \tag{6}$$

where $\Delta R(t)$ is the change in the recorded signal. In our proposed CWC technique, magnitude-squared coherence (MSC) is used, which estimates the strength of the relationship between two random variables in the frequency domain.

In our case, MSC is used to describe the similarity between two waveforms recorded at different levels of stress: Y_0 is the reference waveform recorded at the initial stress condition of the material and Y_i is a waveform recorded at a certain level of interior stress, σ_i . The cross-spectrum $[R_{Y_0Y_i}(e^{j\omega})]$ of any two signals is a complex function of ω , and the normalized cross-power spectrum is known as the coherence function [31]:

$$\text{MSC} = \left| C_{Y_0Y_i}(e^{j\omega}) \right|^2 = \frac{|R_{Y_0Y_i}(e^{j\omega})|^2}{R_{Y_0}(e^{j\omega})R_{Y_i}(e^{j\omega})} \quad (7)$$

By assuming $\Delta R(t)$ can be represented by MSC at the pulse wavelength, λ , Eq. (7) can be reformulated as:

$$\text{MSC}(\lambda) \propto M(\lambda, A)\Delta\sigma \quad (8)$$

where M is a constant that represents the slope of the linear relationship between the MSC and $\Delta\sigma$. This constant is also function of the wavelength (λ) of the source and the aggregate effect (A) for a specific specimen or member. Small wavelengths are more sensitive to micro cracks and relocation of the aggregates and the maximum size of the aggregate influences the interaction of the ultrasonic wave with the aggregates, which is discussed in section ‘‘Laboratory Experiments’’. MSC takes values between one and zero. If Y_0 is equal to Y_i , the MSC value is equal to one, which implies there is no difference between the signals; otherwise, it is less than one and greater than or equal to zero. In other words, a value of one indicates a perfect match while decreasing values correspond to decreasing similarity between signals. Also, the M value has always a negative sign because the MSC decreases from one at the initial condition with increasing internal stress [25].

For comparison, the change in the recorded ultrasonic signal, $\Delta R(t)$ can be estimated by using the coefficient of determination, R^2 , which is also referred to as the squared correlation coefficient, ρ^2 . The correlation coefficient is also known as the Pearson correlation coefficient and represents a measure of the strength of the relationship between two random variables by using linear regression [32]. It can be calculated by using:

$$\rho_{Y_0, Y_i} = \rho = \frac{\text{COV}(Y_0, Y_i)}{\sigma_{Y_0}\sigma_{Y_i}} = \frac{\sigma_{Y_0, Y_i}}{\sigma_{Y_0}\sigma_{Y_i}} \quad (9)$$

$$R^2 = \rho^2 = M(\lambda, A)\Delta\sigma \quad (10)$$

Since the coefficient of determination estimates the difference between the signals in the time domain, estimating the time lag between the signals is critical. For this purpose, cross correlation was applied on the full waveform signals by using Eq. (1). The waveforms were adjusted by shifting each signal

by its time lag before calculating R^2 , resulting in what we refer to as the adjusted coefficient of determination, $R^{2'}$.

4 Laboratory Experiments

For all experiments, we utilized two Panametrics V103 normal-wave transducers, using one as a transmitter (T) and the other one as a receiver (R), as illustrated in Fig. 1. The transmitter was connected to a BK Precision 4053 arbitrary waveform generator, which produced a 100 or 50 kHz Morlet-type pulse (see Fig. 6) at 20 Vpp. These frequencies have been reported in the literature (see e.g., Fröjd and Ulriksen [33]) and were found suitable for our experiments as well. Both transducers were coupled to the concrete using hot glue and connected to a high-speed data recorder (Elsys TraNET FE) to record both the transmitted and recorded waveforms. The recorder triggered on the transmitted signal in order to record 32,768 samples at a sampling rate of 10 MHz (with 500 kHz low-pass anti-aliasing filters), which ensured that both the coherent as well as the coda portions of the recorded waveforms were fully captured. The number of pre-trigger samples equaled 10% of the total number of samples. All laboratory specimens were loaded using a programmable 1112-kN-capacity (250-kip-capacity) hydraulic concrete cylinder compression-testing machine (Forney LP) with a loading rate of 0.156 kN/s (35 lb/s).

4.1 Test Specimens and Loading Protocols

4.1.1 Test 1: Monotonically-Loaded Cylinder

The goal of this test was to evaluate if the proposed CWC technique is able to capture an applied compressive stress and to investigate the aggregate effect on the results by varying maximum aggregate size. For this purpose, two concrete cylinders (152 × 305 mm (6 × 12 in)) were cast and tested, and found to exhibit a similar ultimate stress. However, each cylinder had a different maximum aggregate size. These cylinders were named as Specimen C1 and C2. In this test, the cylinders were monotonically loaded in compression up to failure. A pitch-catch setup (illustrated in Fig. 1) was used during loading and is shown in Fig. 2. The transducers were attached at mid-height of the cylinders. A pulse with a 100 kHz central frequency was used with a pulse repetition frequency (PRF) of 31.74 Hz to ensure high-resolution continuous monitoring and compatibility with the data acquisition unit on the compression machine.

4.1.2 Test 2: Stepwise-Loaded Prism

The goal of this test was to investigate the effect of pulse frequency (or wavelength, λ) on the results of the CWC, as

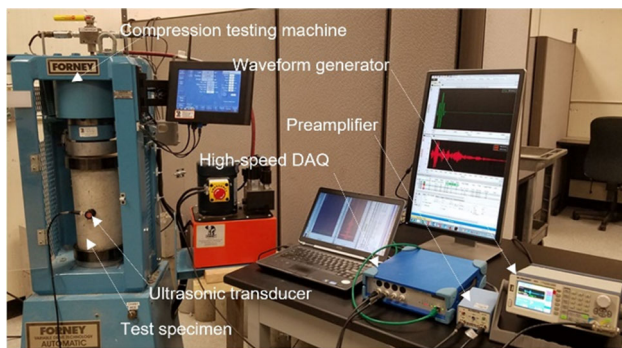


Fig. 2 Photo of experimental test setup for Test 1

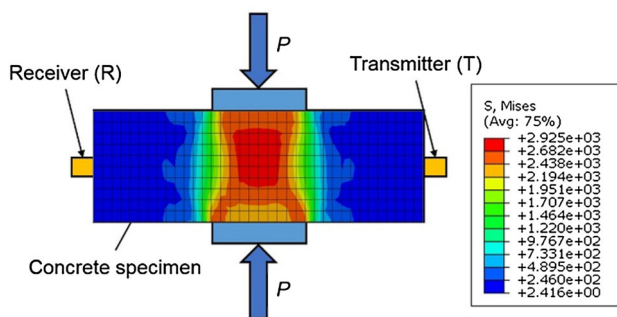


Fig. 3 Illustration of experimental setup for Test 2 and the results of FE simulation at an applied load, $P = P_{ult}$ (Color figure online)

well as to show the ability of the CWC technique to detect changes in internal stresses when the transducers are attached to an unstressed surface. In this test, two concrete prisms with the same dimensions of $152 \times 152 \times 533$ mm ($6 \times 6 \times 21$ in) were used, coming from the same batch. They were partially loaded about the centerline on a 152×152 mm (6×6 in) loading area and the same pitch-catch and setup as used in Test 1 was employed, as illustrated in Fig. 3. The result of a finite element (FE) simulation for this specimen showed that the stresses at the location of the transducers are near zero at the ultimate load level, as shown in Fig. 3. The first prism (P1) was loaded up to 40% of ultimate stress by four loading steps where each load increment equaled 10% of ultimate stress. During each loading step, the load was held and six pulses were transmitted: three at 50 kHz and three at 100 kHz. The second prism (P2) was loaded up to 80% of ultimate stress. Like the first prism, the load was increased in steps and each step equaled 10% of ultimate stress. Three pulses at 100 kHz were transmitted during load holding.

4.2 Results

4.2.1 General Observations

As expected, the recorded waveforms were found to be longer and more complicated than the transmitted pulse due to the

heterogeneity of the concrete and specimen size. Figure 4a shows three waveforms recorded at different levels of applied stress for Specimen C2.

It can be observed that not all portions of the wave are affected the same way by an applied stress. The earlier (coherent) portion of the waveform (Fig. 4b) is less affected by changes in applied stress than the later (coda) portion (Fig. 4c). The coherent portion does not show any noticeable change due to the increase of the applied stress in low stress cases (up to 40% of ultimate stress). A phase shift is only apparent at the 80% of ultimate stress level. Figure 5 confirms that there is no change in the time of flight (TOF), which considers only the coherent portion of the waveform, until approximately 70% of ultimate stress (vertical dashed line) is reached. This explains why traditional techniques, for instance the pulse velocity test [34], are not capable of capturing changes in applied stress under service-level conditions.

On the other hand, the coda wave portion shows high sensitivity to changes in applied stress for any level (Fig. 4c) where these changes appear as changes in amplitude, frequency, and time shift. Figure 6, in addition to showing the transmitted pulse in the time domain (Fig. 6a), also shows examples in the frequency domain (Fig. 6b) of the three recorded signals presented in Fig. 4. Although the recorded waveforms contain the same range of frequencies as the transmitted pulse, each recorded wave showed an uneven attenuation in this range of frequencies due to the nonlinearity of concrete response as shown in Fig. 6b. In addition, this attenuation was influenced by the load (stress) level, but the relationship between the load level and amount of the attenuation could not be extracted directly. Therefore, MSC was used to determine and evaluate the changes in the recorded wave (in the frequency domain) due to the stress effects.

In order to evaluate the noise of the system on the MSC calculations, 100 pulses were transmitted at the zero stress level in all specimens and evaluated. The error in the MSC value was found to be 0.0003; therefore, the system's noise can be neglected. This also proved that the decrease in the MSC value is a result of the change of applied stress.

4.2.2 Test 1: Monotonically-loaded Cylinder

Results of Different Waveform Comparison Parameters

The ultimate stress of Specimen C1 was 24.1 MPa (3500 psi), which is a typical concrete strength used in reinforced concrete structures. For correlating the applied stress and the changes in the recorded waveforms, Eqs. (8) and (10) were applied and the results are presented in Fig. 7a. The results show that both R^2 and $MSC(\lambda)$ are a function of applied stress, and exhibit a linear relationship up to 30% of ultimate stress. After this limit, the time shift between the full waveforms has a large influence on the results of R^2 ,

Fig. 4 Three samples of recorded waveforms from Specimen C2 for different levels of applied stress. **a** Entire recorded waveforms. **b** Sample window from the coherent portion. **c** Sample window from the coda portion (Color figure online)

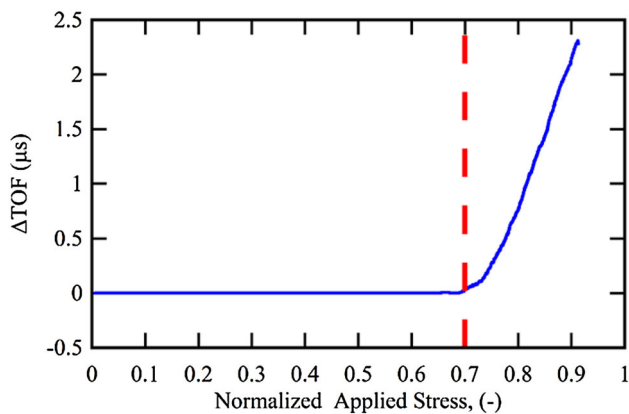
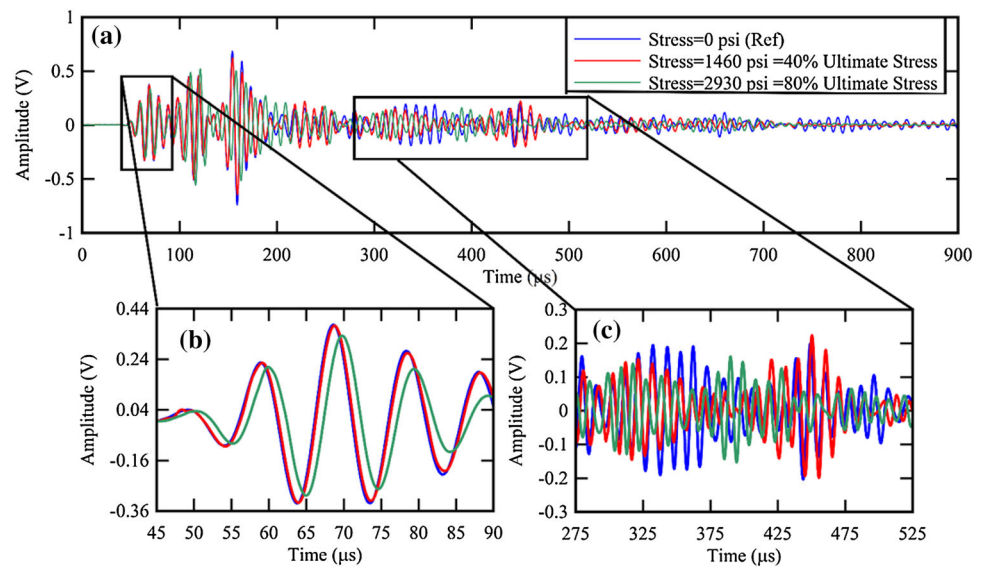


Fig. 5 Δ TOF versus normalized stress for specimen C2

since the R^2 compares between signals in the time domain. This time shift was calculated for full waveforms by using Eq. (1), and the results are presented in Fig. 7b. To conclude, the R^2 is more sensitive at higher stress levels compared to $MSC(\lambda)$ due to its sensitivity to the observed time shift in the recorded waveforms. In order to exclude the effect of time shift, the signals were shifted in the time domain, to produce the adjusted coefficient of determination ($R^{2'}$). The results of $R^{2'}$ match the $MSC(\lambda)$ curve almost perfectly, as can be seen in Fig. 7a. In conclusion, the results of $MSC(\lambda)$ and R^2 are the same after excluding the time shift in the signals.

Some recorded signals showed a superposition between the pulse response and spontaneous acoustic emissions due to the imposed loading, which had an unwanted influence on the results of R^2 . In order to exclude the signals that contained the acoustic emission (AE) hits, the energy filter presented in [7] was applied to all recorded signals. On the other hand, AE hits did not affect the $MSC(\lambda)$'s results. Therefore, only the $MSC(\lambda)$ results are presented and discussed subsequently.

Influence of Mechanical Properties The ultimate stress of concrete cylinder Specimens C1 and C2 was 25.3 and 24.1 MPa (3670 and 3500 psi), respectively. Figure 8a shows the relationship between $MSC(\lambda)$ and normalized applied stress for these two concrete cylinders and one specimen from tests described in [25]. These specimens were tested using the same experimental setup, pulse frequency, and reached approximately the same compressive strength, but had different maximum aggregate sizes. The results show a linear relationship between $MSC(\lambda)$ and applied stress up to approximately 55% of ultimate stress. In addition, each specimen has a particular slope M , for the linear portion of the $MSC(\lambda)$ -applied stress relationship. In Fig. 8b it can be observed that the $MSC(\lambda)$ curves were similar in the linear portion for specimens (up to 55% of ultimate) with the same aggregate size and for varying compressive strengths ranging from 22.6 to 29.1 MPa (3280 to 4220 psi). To conclude, the slope of the linear portion is mainly influenced by the maximum aggregate size and not by compressive strength.

Effect of Sampling Frequency A relatively high sampling frequency is required when working with ultrasonic waves in concrete since typical pulse frequencies are in the range of 20–150 kHz. As discussed earlier, this pulse frequency range is suitable for monitoring the changes of the diffuse portion of signals from concrete [33]. Using a high sampling frequency, however, increases the amount of data and requires high-speed data acquisition systems, thus increasing the overall computational cost, which can become prohibitive in a field setting. Decreasing the sampling frequency from 10 MHz to 500 kHz using by numerical downsampling does not influence the $MSC(\lambda)$ results as shown in Fig. 9, which is demonstrated by the perfect match between them. To conclude, CWC is able to capture changes with relatively low

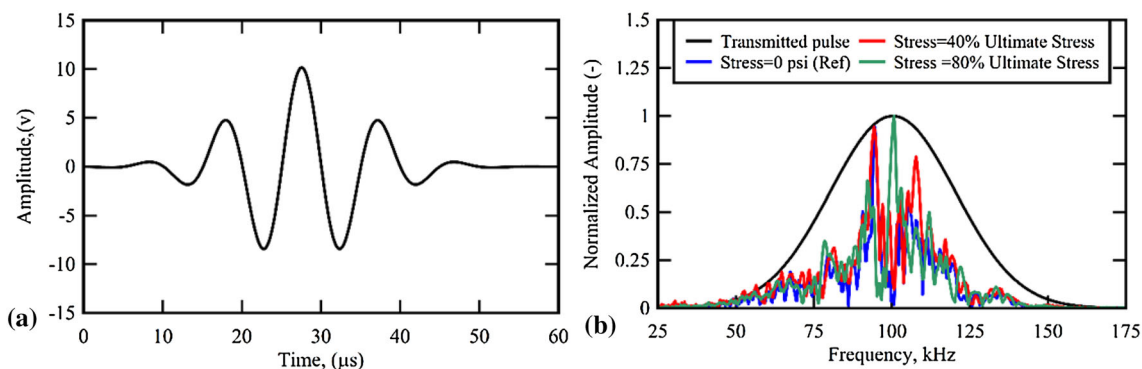


Fig. 6 **a** Transmitted pulse in the time domain. **b** Waveforms in frequency domain: transmitted pulse and three recorded waveforms at different levels of applied stress. The recorded waveforms were normalized according to the maximum spectra amplitude of the reference signal (blue curve) (Color figure online)

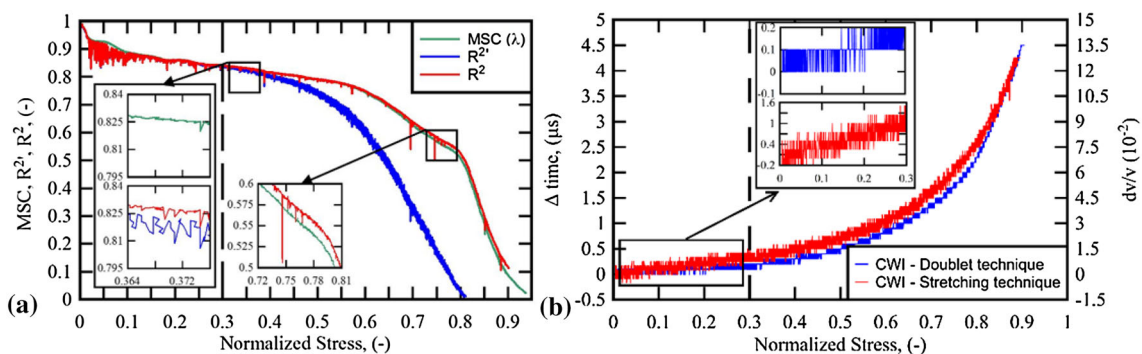


Fig. 7 Different waveform comparison parameters versus normalized applied stress for specimen C2. **a** $MSC(\lambda)$, R^2 , and $R^{2'}$ versus normalized stress. **b** Time shift (doublet technique) and dv/v (stretching technique) versus normalized stress (Color figure online)

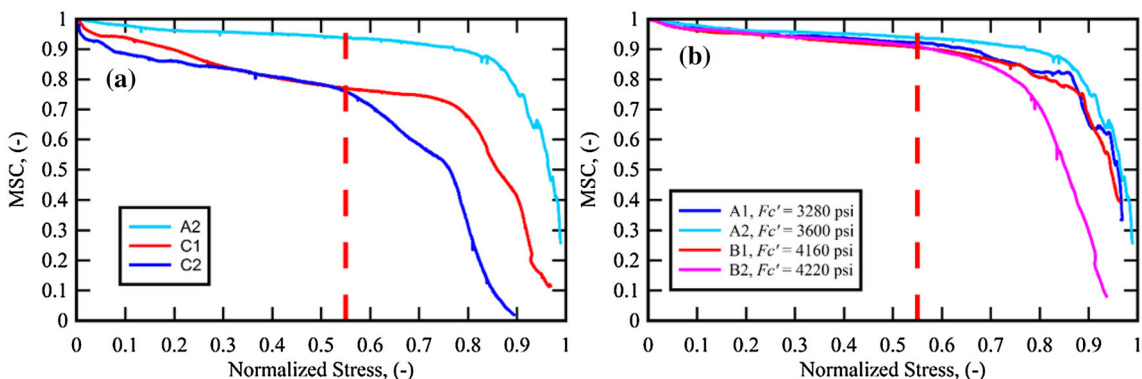


Fig. 8 $MSC(\lambda)$ versus normalized applied stress. **a** Varying maximum aggregate size. **b** Varying compressive strength [25] (Color figure online)

sampling frequencies, without the need for post-acquisition oversampling.

Linear Regression A linear regression curve-fit with 95% confidence intervals was applied to the results of Specimens C1 and C2 over the range of 0 to 55% of ultimate stress, as shown in Fig. 10. It can be observed that all data points are in range of the prediction intervals. The confidence intervals are not shown because the large number of samples, which effectively collapses them onto the fitted line. It can be observed

that a moderate linear relationship exists between $MSC(\lambda)$ and applied stress where the R^2 for the linear fit for Specimens C1 and C2 is equal to 0.987 and 0.993, respectively. In addition, the root-mean-square error (RMSE) was negligible for both specimens and the p value was zero for all specimens, as shown in Table 1, which indicates the high statistical relationship.

This demonstrates that Eq. (8) is applicable for relating the changes in applied stress with changes in the coda wave for

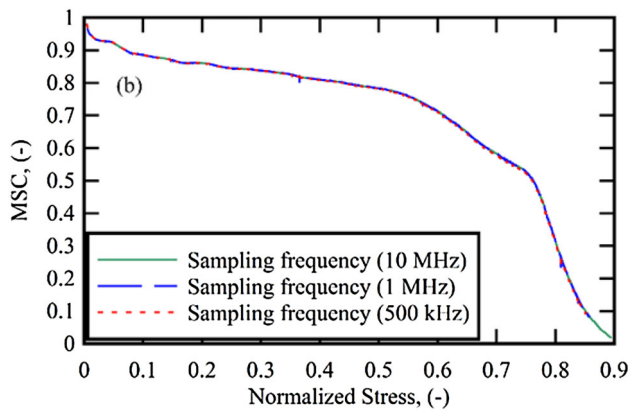


Fig. 9 Effect of decreasing the sampling frequency on the CWC results for specimen C2

the stress range of approximately 0–55% of ultimate stress. Beyond that value, the time shifts have an over-proportional effect on the changes in the recorded waveform. Table 1 shows the results of using the CWC technique by applying Eq. (8), and presents the computed test coefficient, M .

4.2.3 Test 2: Stepwise-Loaded Prism

For the concrete prisms, nine $MSC(\lambda)$ values were obtained at each load level, consisting of three pulses with the same wavelength. The variance of these values was found very small, as shown in Fig. 11. Also, there was no noise effect from either inside or outside the system since the calculation of $MSC(\lambda)$ depends on the frequency of the recorded waveforms. This test demonstrates that changes in the interior stress can be detected using our proposed CWC technique

when the changes are within the propagation path of the wave. Changes in the interior stress do not have to extend to the surface to which the transducers are attached (see Fig. 3), which is an advantage compared to sensors that are attached to the surface such as strain gauges. The results of the first prism (P1) show that the sensitivity of the $MSC(\lambda)$ values was influenced by the wavelength, which is a function of pulse frequency assuming a p-wave velocity of 3600 m/s (141,000 in/s). The pulse with the smaller wavelength was more sensitive to changes in interior stress than the larger wavelength, as shown in Fig. 11a, b. When the applied load increased from 10 to 40% of ultimate stress, the $MSC(\lambda)$ decreased from 0.88 to 0.6 for $\lambda = 36$ mm (1.41 in), where decrease for $\lambda = 66$ mm (2.62 in) was from 0.88 to 0.85. Moreover, the R^2 of the linear fit for the results of the $MSC(\lambda)$ for the shorter wavelength was higher, as shown in Table 2.

For Specimen P2 (see Fig. 11c), the results show the high sensitivity of the $MSC(\lambda)$. Increasing the applied load from 10 to 80% from ultimate stress, the $MSC(\lambda)$ decreased from 0.78 to 0.2. The sensitivity of this test is very close to the sensitivity of Specimen P1 due to wavelength similarity in both cases. The results also show that the relationship is linear between the change in the $MSC(\lambda)$ value and the change in the applied stress, as shown in Fig. 11c. Although the linear fit for the results shows one slight deviation at a load of 60% of ultimate, $R^2 = 0.988$, as shown in Table 2. The relationships are statistically highly significant with near-zero p-values.

4.2.4 Final Remarks Regarding Laboratory Tests

The $MSC(\lambda)$ curves typically show a sharp drop at the initial loading phase. This phenomenon appears only in a

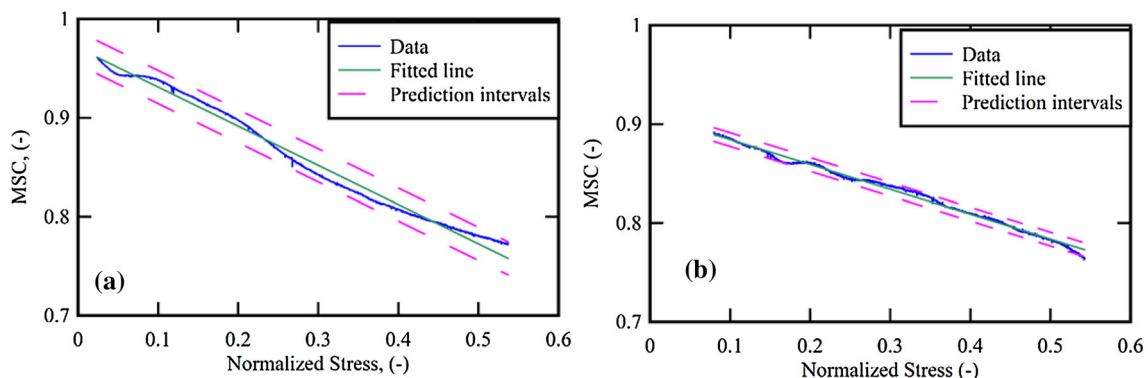


Fig. 10 Results of the linear regression for $MSC(\lambda)$ versus normalized applied stress. **a** Specimen C1. **b** Specimen C2 (Color figure online)

Table 1 Regression results for specimens C1 and C2

Specimen	Max. size of aggregate (in)	M	R^2	p-value	RMSE	SE	Numbers of samples
C1	1/2	-0.3963	0.987	0	0.00683	0.00116	1692
C2	7/16	-0.2513	0.993	0	0.00283	0.00055	1500

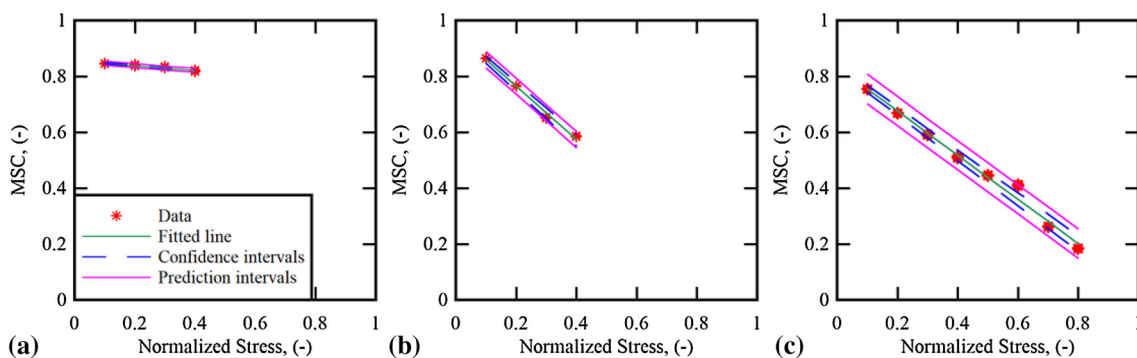


Fig. 11 MSC(λ) versus normalized applied stress for specimens P1 and P2. **a** Specimen P1, $\lambda = 66$ mm (2.61 in). **b** Specimen P1, $\lambda = 36$ mm (1.41 in). **c** Specimen P2, $\lambda = 36$ mm (1.41 in) (Color figure online)

Table 2 Regression results for concrete prisms

Specimen	Wavelength (in)	M	R^2	p-value
P1	2.61	-0.06991	0.62	1.24e-08
P1	1.41	-0.9496	0.99	1.12e-35
P2	1.41	-0.7895	0.988	2.07e-68

laboratory setting when a hydraulic machine is used to apply the load. It is likely associated with the initial contact of the loading cap and settling and in some regard another testament to the sensitivity of our proposed approach.

5 Field Test

5.1 Description of Load Test

The objective of the field test was to demonstrate our proposed CWC technique’s sensitivity to capturing internal changes in tensile and compression stresses in real structural

concrete members. A prestressed concrete bridge located on the I-84 Highway near Echo, Oregon undergoing in-service load testing was selected for this purpose. The bridge consists of three non-continuous spans with lengths of 12.2, 24.4, and 12.2 m (40, 80, and 40 ft.). The superstructure of the bridge is made of prestressed concrete girders and a reinforced concrete deck slab as shown in Fig. 12a, b. This bridge is part of the FHWA Long-Term Bridge Performance (LTBP) program where 42 sensors were already mounted for monitoring the long-term performance of the bridge. In July 2017, FHWA calibrated the monitoring system by performing an in-service load test (see Fig. 12c) and invited us to participate.

Loaded water tank and dump trucks were used and weight information are listed in Table 3. During the loading process, a pitch-catch setup was used to capture changes in applied stress in one interior girder (Fig. 12d) that was a part of the external span. Additionally, the stress in one of the bent’s columns was monitored (see Fig. 12a). Consistent with the type of structural member, the tests are subsequently referred to as girder test and column test. The same data acquisition setup used for the laboratory tests was used. Power was provided by large uninterruptable power supply (UPS) device

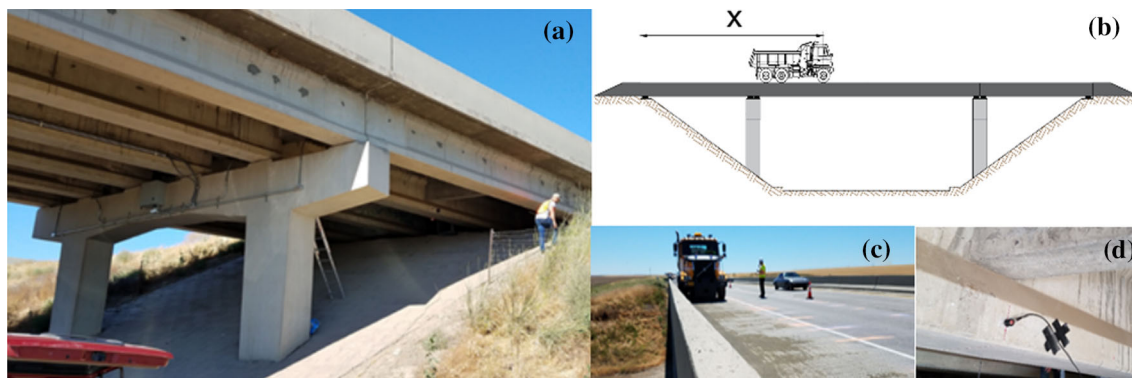


Fig. 12 In-service load test on I-84 Bridge near Echo, Oregon. **a** Photo from road under the bridge showing bent and girders. **b** Elevation view with test truck. **c** Photo of deck with approaching test truck. **d** Photo of girder with ultrasonic transducer

Table 3 Weight information for test trucks

Truck	Axle					
	Steer		Tandem			
			Front axle		Rear axle	
	Weight (kN) (lbs)	Distance (m) (in)	Weight (kN) (lbs)	Distance (m) (in)	Weight (kN) (lbs)	Distance (m) (in)
ODOT water truck	77.8	0	81.0	5.28	79.2	6.66
	17,500	0	18,200	208	17,800	262
ODOT dump truck	71.8	0	75.2	4.47	72.7	5.79
	16,150	0	16,900	176	16,350	228

Table 4 Truck stop locations for girder test (see Fig. 12b)

Stop case	1	2	3	4	5	6	7	8	9	10	11	12	13
Steer axle position, x (m) (ft)	36.6 120	37.8 124	39.0 128	39.6 130	41.5 136	42.7 140	44.5 146	45.7 150	47.5 156	48.8 160	50.6 166	53.6 176	54.9 180

Table 5 Truck stop locations for column test (see Fig. 12b)

Stop case (interior span)	1	2	3	4	5	6	7	8	9
Steer axle position, x (m) (ft)	12.2 40	15.2 50	18.3 60	20.1 66	23.2 76	25.0 82	28.7 94	32.3 106	36.0 118
Stop case (exterior span)	10	11	12	13	14	15	16	17	
Steer axle position, x (m) (ft)	39.0 128	39.6 130	41.5 136	44.5 146	45.7 150	48.8 160	50.6 166	53.6 176	

battery connected to a fuel-powered generator. The UPS device also ensured a clean power signal.

For the girder test, the transmitting and receiving transducers were attached to the mid-thickness of the bottom flange at the centerline of the girder (see Fig. 12d). A water tank truck crossed the bridge starting from the beginning of the right exterior span with 13 stop points, as shown in Table 4. Throughout the loading process, which consisted of moving and stopping of the truck, a 50 kHz Morlet-type pulse was sent from the transmitter every 20 ms and recorded at a sampling frequency of 10 MHz. This test was performed twice.

For the column test, the transducers were located at the mid-height of the column in the short direction, which was 0.91 m (36 in), as illustrated in Fig. 12a. A water tank truck and dump truck side-by-side crossed the interior span (24.4 m (80 ft span)) nine times and the exterior span (12.2 m (40 ft)) eight times as shown in Table 5. Because of the difficulty of making the trucks moving and stopping together, the dump truck was moved first and stopped at a stopping point and waiting for the water tank truck to catch up. In this test, a 50 kHz Morlet-type pulse was used as well. The pulse repetition frequency and sampling frequency was 3 Hz and 3.3 MHz, respectively.

5.2 Results and Discussion

The results of the $MSC(\lambda)$ of these tests as a function of test time are presented in Fig. 13. The thirteen and the seventeen stops of the trucks can be distinguished in this figure for both girder and column tests, respectively. In addition, several sharp drops in the $MSC(\lambda)$ curve (highlighted with red circles) can be observed that occur when the truck arrives at a stop location. This phenomenon is likely related to the transient vibrations induced by the truck when the driver hits the brakes to stop. Using a pulse with 50 kHz central frequency was found suitable to monitor the change in applied stress due to the weight of the trucks, where the $MSC(\lambda)$ varied between 1.0 (unloaded) to 0.57 and 0.3 (maximum load) for column and girder tests, respectively. The column test and previous tests presented in this paper demonstrate the capability of the proposed CWC technique to monitor minute changes in compression stresses. Additionally, the girder test shows the same the capability to sense a change in tension stresses. Unfortunately, no deformation measurements were available for direct comparison. An estimate of the maximum tensile strain in the girder during loading is $10 \mu\epsilon$. This was confirmed as a reasonable value with the bridge owner and based on readings available at other locations.

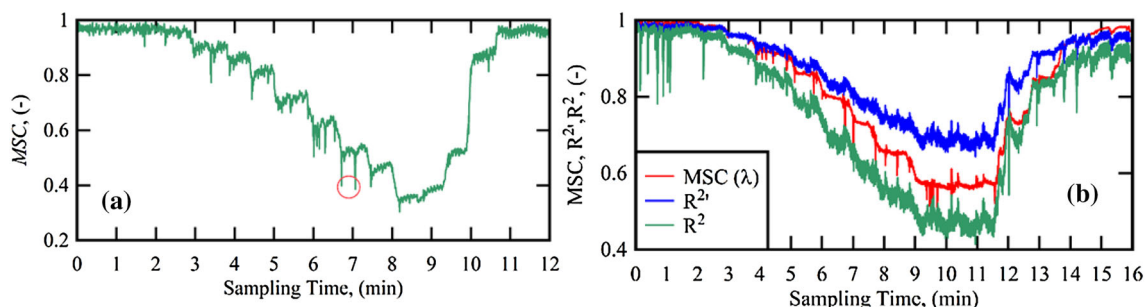


Fig. 13 $MSC(\lambda)$ versus test time. **a** Girder test. **b** Column test. Red circles indicate drops in the $MSC(\lambda)$ curve when the test trucks arrived at a stop location (Color figure online)

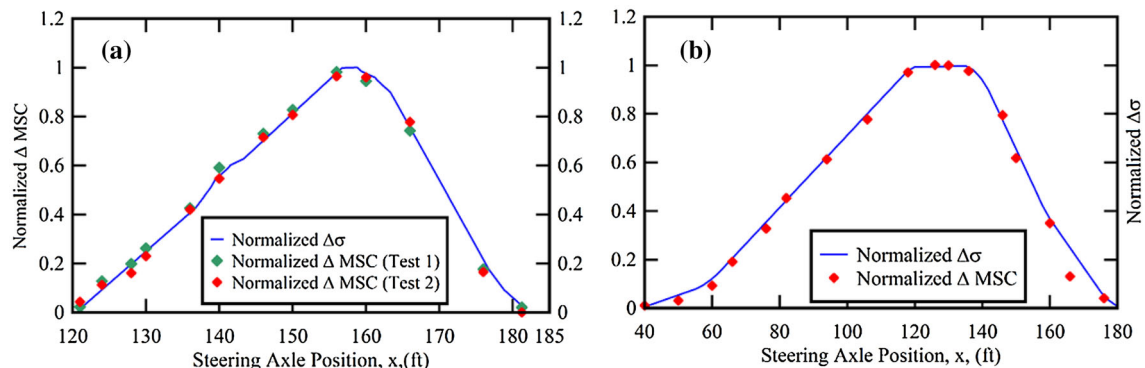


Fig. 14 Normalized $MSC(\lambda)$ versus steering axle position. **a** Girder test. **b** Column test (Color figure online)

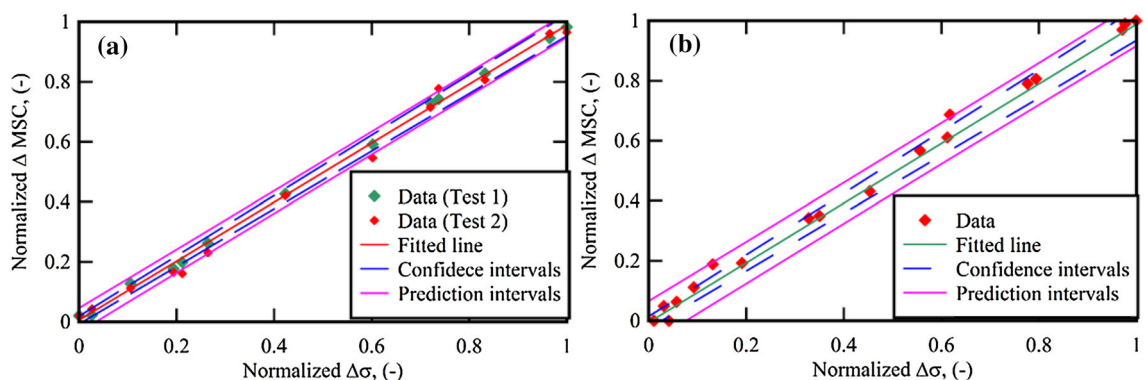


Fig. 15 Normalized $MSC(\lambda)$ versus normalized $\Delta\sigma$. **a** Girder test. **b** Column test (Color figure online)

Since the truck is a moving load, the influence line can be used to correlate changes in the internal force and corresponding stresses at that location of the bridge with respect to the truck position. Therefore, the influence line for the bending moment in the girder and the axle force in column for each truck stop location were computed using a conventional moving load analysis. From the influence line for the bending moment, the influence line of the change in tensile force in the bottom flange of the girder was obtained. The influence line of the change in compression force in the column was determined from the influence line for the steer truck axle load. Figure 14 shows the normalized change in stress (col-

umn and girder bottom flange) and the normalized change in $MSC(\lambda)$. The results show that the $MSC(\lambda)$ values correlate very well with changes in the internal stresses, which demonstrates the ability of the proposed CWC technique to capture minute changes in internal stress. The $MSC(\lambda)$ results for the two girder tests were in excellent matching, as shown in Fig. 14a, indicating robustness of the CWC’s results. Moreover, CWC can monitor the unloading cases, when the truck passes the maximum stress location. Finally, for the girder test, it can be observed that the $MSC(\lambda)$ value returns to the original value as shown in Figs. 13a and 14a, indicating that no residual stress or damage has occurred due to the loading.

For the column test, the residual stress could not be investigated because the DAQ ran out its storage memory capacity to complete the test.

Linear regression curve-fits with 95% confidence intervals were applied to the results to estimate the accuracy of the CWC technique. Figure 15 shows that all $MSC(\lambda)$ results for the column and girder tests are located in the confidence interval limits except for two points of the column test. However, these two points are still located within the prediction intervals. Additionally, a linear relationship between the $MSC(\lambda)$ results and applied stress can be assumed, since the coefficients of determination R^2 , are equal to 0.996 and 0.999 for column and girder tests, respectively, and the root mean square error RMSE, for the column and girder tests are equal to 0.0249 and 0.0129, respectively. Finally, the p-values were found to be near zero, indicating that statistically significant relationship exists.

6 Conclusions

The results presented in this paper demonstrate the ability of our proposed CWC technique to relate changes in an ultrasonic stress wave to changes that occur in concrete due to internal stresses. In the proposed technique, a wave similarity parameter based on magnitude-squared coherence evaluated at a specific wavelength, $MSC(\lambda)$ is used to measure the similarity between recorded ultrasonic waveforms in their frequency domain. Similarly, the time-shift-adjusted squared correlation coefficient, R^2 produces the same results as $MSC(\lambda)$. Both $MSC(\lambda)$ and R^2 show a linear relationship with the applied stress up to a specific limit which depends on a number of variables but can be assumed to be at least 50% of ultimate stress. Linear regression produced a test constant, M , which represents the slope of the $MSC(\lambda)$ versus applied stress relationship, and can thus be interpreted as a measure of sensitivity. The results showed that M depends on the maximum size of the aggregate more than the compressive strength of concrete, in addition to the dependence on the wavelength of the transmitted pulse. The sensitivity of the $MSC(\lambda)$ parameter increased with decreasing wavelength. The proposed CWC technique was also validated in a field setting where it was found to correlate extremely well with the internal stresses at the sensor locations. The CWC technique exhibits two advantages over the more established coda wave interferometry (CWI) approach and traditional deformation measurements such as strain gauges. First, no arbitrary windows need to be selected for CWC since the entire waveform is used. Second, using a sampling frequency equal to five times the pulse frequency is good enough to produce accurate relations between $MSC(\lambda)$ and applied stress. Finally, compared to traditional deformation sensors, ultrasonic monitoring using the CWC technique can measure

changes in the internal stress that are not observable on the surface of a member. Future work includes evaluating the technique's ability to measure residual stresses and other changes such as deterioration mechanisms.

Acknowledgements We would like to acknowledge the financial support from the Higher Committee of Education Development in Iraq (HCED), which funded the first author, and the Department of Civil and Environmental Engineering at Portland State University for providing laboratory equipment and specimens. Finally, we thank Mr. Salih Mahmood for assisting with the finite element model illustrated in Fig. 3.

References

- Zhang, Y., Planès, T., Larose, E., Obermann, A., Rospars, C., Moreau, G.: Diffuse ultrasound monitoring of stress and damage development on a 15-ton concrete beam. *J. Acoust. Soc. Am.* **139**, 1691–1701 (2016). <https://doi.org/10.1121/1.4945097>
- Zhang, Y., Abraham, O., Grondin, F., Loukili, A., Tournat, V., Duff, A., Le, L., Lascoup, B., Durand, O.: Study of stress-induced velocity variation in concrete under direct tensile force and monitoring of the damage level by using thermally-compensated Coda Wave Interferometry. *Ultrasonics* **52**, 1038–1045 (2012). <https://doi.org/10.1016/j.ultras.2012.08.011>
- Hughes, D.S., Kelly, J.L.: Second-order elastic deformation of solids. *Phys. Rev.* **92**, 1145–1149 (1953). <https://doi.org/10.1103/PhysRev.92.1145>
- Murnaghan, F.D., Murnaghan, B.F.: Finite deformations of an elastic solid. *Am. J. Math.* **59**, 235–260 (1937).
- Planès, T., Larose, E.: A review of ultrasonic Coda Wave Interferometry in concrete. *Cem. Concr. Res.* **53**, 248–255 (2013). <https://doi.org/10.1016/j.cemconres.2013.07.009>
- Stähler, S.C., Sens-Schönfelder, C., Niederleithinger, E.: Monitoring stress changes in a concrete bridge with coda wave interferometry. *J. Acoust. Soc. Am.* **129**, 1945–1952 (2011). <https://doi.org/10.1121/1.3553226>
- Hafiz, A., Schumacher, T.: Monitoring of applied stress in concrete using ultrasonic full-waveform comparison techniques. In: *Nondestructive Characterization and Monitoring of Advanced Materials, Aerospace, and Civil Infrastructure 2017*. p. 101692Z. International Society for Optics and Photonics (2017)
- Grêt, A., Snieder, R., Scales, J.: Time-lapse monitoring of rock properties with coda wave interferometry. *J. Geophys. Res.* (2006). <https://doi.org/10.1029/2004jb003354>
- Legland, J.-B., Zhang, Y., Abraham, O., Durand, O., Tournat, V.: Evaluation of crack status in a meter-size concrete structure using the ultrasonic nonlinear coda wave interferometry. *J. Acoust. Soc. Am.* **142**, 2233–2241 (2017). <https://doi.org/10.1121/1.5007832>
- Snieder, R.: The theory of coda wave interferometry. *Pure Appl. Geophys.* **163**, 455–473 (2006). <https://doi.org/10.1007/s00024-005-0026-6>
- Payan, C., Quiviger, A., Garnier, V., Chaix, J.F., Salin, J.: Applying diffuse ultrasound under dynamic loading to improve closed crack characterization in concrete. *J. Acoust. Soc. Am.* **134**, 211–216 (2013). <https://doi.org/10.1121/1.4813847>
- Larose, E., Obermann, A., Digulescu, A., Planès, T., Chaix, J.-F., Mazerolle, F., Moreau, G.: Locating and characterizing a crack in concrete with diffuse ultrasound: a four-point bending test. *J. Acoust. Soc. Am.* **138**, 232–241 (2015)
- Bui, D., Kodjo, S.A., Rivard, P., Fournier, B.: Evaluation of concrete distributed cracks by ultrasonic travel time shift under an external mechanical perturbation: study of indirect and semi-direct

- transmission configurations. *J. Nondestr. Eval.* **32**, 25–36 (2013). <https://doi.org/10.1007/s10921-012-0155-7>
14. Schurr, D.P., Kim, J.Y., Sabra, K.G., Jacobs, L.J.: Damage detection in concrete using coda wave interferometry. *NDT & E Int.* **44**, 728–735 (2011). <https://doi.org/10.1016/j.ndteint.2011.07.009>
 15. Moradi-Marani, F., Kodjo, S.A., Rivard, P., Lamarche, C.-P.: Effect of the temperature on the nonlinear acoustic behavior of reinforced concrete using dynamic acoustoelastic method of time shift. *J. Nondestr. Eval.* **33**, 288–298 (2014). <https://doi.org/10.1007/s10921-013-0221-9>
 16. Schurr, D.P., Kim, J.Y., Sabra, K.G., Jacobs, L.J.: Monitoring damage in concrete using diffuse ultrasonic coda wave interferometry. In: *AIP Conference Proceedings*. pp. 1283–1290 (2011)
 17. Shokouhi, P.: Stress-and damage-induced changes in coda wave velocities in concrete. In: *AIP Conference Proceedings*. pp. 382–389. AIP (2013)
 18. Shokouhi, P., Niederleithinger, E., Zoëga, A., Barner, A., Schöne, D.: Using ultrasonic coda wave interferometry for monitoring stress induced changes in concrete. *Symp. Appl. Geophys. Eng. Environ. Probl.* **2010**, 650–654 (2010). <https://doi.org/10.4133/1.3445493>
 19. Larose, E., Hall, S.: Monitoring stress related velocity variation in concrete with a 2×10^{-5} relative resolution using diffuse ultrasound. *J. Acoust. Soc. Am.* **125**, 1853–1856 (2009)
 20. Jiang, H., Zhang, J., Jiang, R.: Stress evaluation for rocks and structural concrete members through ultrasonic wave analysis. *J. Mater. Civ. Eng.* **29**, 4017172 (2017)
 21. Liu, S., Zhu, J., Wu, Z.: Implementation of Coda Wave Interferometry Using Taylor Series Expansion. *J. Nondestr. Eval.* (2015). <https://doi.org/10.1007/s10921-015-0300-1>
 22. Larose, E., Planès, T., Rossetto, V., Margerin, L.: Locating a small change in a multiple scattering environment. *Appl. Phys. Lett.* doi (2010). <https://doi.org/10.1007/s10921-015-0300-1>
 23. Planès, T., Larose, E., Margerin, L., Rossetto, V., Sens-Schönfelder, C.: Decorrelation and phase-shift of coda waves induced by local changes: multiple scattering approach and numerical validation. *Waves Random Complex Media.* **24**, 99–125 (2014). <https://doi.org/10.1080/17455030.2014.880821>
 24. Niederleithinger, E., Wolf, J., Mielentz, F., Wiggemhauser, H., Pirskawetz, S.: Embedded ultrasonic transducers for active and passive concrete monitoring. *Sensors.* **15**, 9756–9772 (2015). <https://doi.org/10.3390/s150509756>
 25. Hafiz, A., Schumacher, T.: Characterizing the effect of applied stress in concrete by magnitude-squared coherence of ultrasonic full-waveforms. In: *Structural Health Monitoring 2017: Real-Time Material State Awareness and Data-Driven Safety Assurance- Proceedings of the 11th International Workshop on Structural Health Monitoring, IWSHM 2017* (2017)
 26. Grosse, C.: *Quantitative zerstörungsfreie Prüfung von Baustoffen mittels Schallemissionsanalyse und Ultraschall* (1996)
 27. Chen, A., Schumacher, T.: Characterization of flaws in structural steel members using diffuse wave fields. In: *AIP Conference Proceedings*. pp. 761–768 (2014)
 28. Fröjd, P., Ulriksen, P.: Detecting damage events in concrete using diffuse ultrasound structural health monitoring during strong environmental variations. *Struct. Health Monit.* **17**, 410–419 (2018). <https://doi.org/10.1177/1475921717699878>
 29. Zhang, Y., Abraham, O., Tournat, V., Le Duff, A., Lascoup, B., Loukili, A., Grondin, F., Durand, O.: Validation of a thermal bias control technique for Coda Wave Interferometry (CWI). *Ultrasonics* **53**, 658–664 (2013). <https://doi.org/10.1016/j.ultras.2012.08.003>
 30. Große, C., Schumacher, T.: Anwendungen der Schallemissionsanalyse an Betonbauwerken. *Bautechnik.* **90**, 721–731 (2013). <https://doi.org/10.1002/bate.201300074>
 31. Manolakis, D.G., Ingle, V.K., Kogon, S.M.: *Statistical and Adaptive Signal Processing: Spectral Estimation, Signal Modeling, Adaptive Filtering, and Array Processing*. McGraw-Hill, Boston (2000)
 32. Cohen, J.: *Statistical power analysis for the behavioral sciences*, <http://books.google.com/books?id=TI0N2IRA09oC&pgis=1> (1988)
 33. Fröjd, P., Ulriksen, P.: Frequency selection for coda wave interferometry in concrete structures. *Ultrasonics* **80**, 1–8 (2017). <https://doi.org/10.1016/j.ultras.2017.04.012>
 34. ASTM C597-02: *Standard Test Method for Pulse Velocity Trough Concrete*. Annual Book of ASTM Standards. pp. 3–6 (2002). <https://doi.org/10.1520/c0597-09>